Journal of Electroanalytical Chemistry 942 (2023) 117570

Contents lists available at ScienceDirect

Journal of Electroanalytical Chemistry

journal homepage: www.elsevier.com/locate/jelechem

Conversion of toxic waste to wealth: Diesel soot carbon electrode for sodium-hybrid capacitor

Bala Krishnan Ganesan [a,1], Higgins M. Wilson [b,1], Sangho Park [c,*], Sang Joon Lee [b], Yun-Sung Lee [a,*]

[a] School of Chemical Engineering, Chonnam National University, Gwangju 61186, Republic of Korea
[b] Department of Mechanical Engineering, Pohang University of Science and Technology, Pohang 37673, Republic of Korea
[c] Department of Battery Engineering, Dongshin University, Naju-si, Jeollanam-do 58245, Republic of Korea

ARTICLE INFO

Keywords:
Sodium hybrid capacitor
All carbon electrode
Diesel soot carbon
Energy storage
Organic electrolyte

ABSTRACT

In recent years, hybrid capacitors have proven to be an efficient technology in storing energy faster and at a higher energy capacity while utilizing a renewable source. Herein, we report diesel soot derived from automobile exhausts as a carbon source for all carbon sodium-ion hybrid capacitors. To achieve this, a simple synthesis method was used, followed by activation to significantly increase its charge storing capabilities. The high porosity of this activated diesel soot carbon allows us to achieve high charge storage capacity both as anode and cathode, while increased graphitization with interlayer expansion by heat-treatment technique allows us to obtain greater rate performance combined with superior cycle stability. As a result, activated diesel soot carbon could earn double the capacity as compared to pure diesel soot carbon with specific capacities of 198 and 78 $mAhg^{-1}$ as anode and cathode, respectively. Full-cell assembly as a hybrid capacitor with carbon as both cathode and anode could deliver a maximum energy density of 97 $Whkg^{-1}$ and a maximum power density of 10,000 Wkg^{-1} with cycle stability for 50,000 cycles. This article emphasizes the waste-to-wealth technique in active materials for energy storage devices more extensively.

1. Introduction

Because of the growing concerns regarding the use of fossil fuels and their effects on the environment, researchers have been inspired to create technologies for efficient energy conversion and storage [1]. Recent breakthroughs in renewable energy sources may provide a sustainable solution to the world's energy issues, but their supply is unpredictable. Thus, energy storage is critical for making the best use of renewable energy resources [2]. In this sense, hybrid capacitors are the most advanced energy storage devices that deliver high power and energy [3-5]. This system is suitable for modern electronics, electric vehicles, space, heavy industry, and much more due to its high energy density comparable to a secondary battery with ultra-high stability. Lithium-ion batteries and hybrid capacitors with high energy output are now used in segments suffering from significant resource limitations and inadequate capacity to satisfy future energy demands [6]. As an alternative to this problem, sodium-ion-based energy technology is considered the most promising replacement for lithium-based technologies due to its abundance and diverse presence.

In recent years, scientific communities have focused on recycling waste and converting it as starting materials for practical applications such as energy storage and generation. For example, waste materials such as waste coffee beans [7,8], banana fibres [9], silk cocoons [9], and various other sources such as chitin [10], soybean protein [11], wood based [12,13] consumed diesel-based derivatives such as diesel soot carbon [14,15] are used as high surface area carbon sources. When used as electrode material for hybrid capacitors, activated carbon derived from these sources tends to show superior performance in capacity, cycle stability and power output. Diesel soot collected from vehicle exhaust is one material that has not yet been thoroughly studied in energy storage devices. One of the main contributors to air pollution is diesel soot particles. Additionally, the sub-micrometre particles pose a severe environmental risk and significantly impact human and animal health [16,17]. Despite constant efforts to reduce the formation of these hazardous particles, the need for novel techniques for recycling diesel soot remains [18]. Diesel soot particles are produced due to incomplete diesel combustion in diesel-powered engines. Their ultimate composition differs depending on their production source. They are, however, mostly made of pure carbon [19] with a graphitic

* Corresponding authors.
E-mail addresses: shpark@dsu.ac.kr (S. Park), leeys@chonnam.ac.kr (Y.-S. Lee).
[1] Authors made equal contribution.

https://doi.org/10.1016/j.jelechem.2023.117570
Received 20 March 2023; Received in revised form 8 May 2023; Accepted 17 May 2023
Available online 23 May 2023

shell-like structure [20]. Previous reports have described diesel soot structures as carbon nanospheres with an average size of 50 nm [14]. These particles were found to agglomerate and form a chain-like morphology. In addition, a previous study has reported the morphology to be similar to carbon nano-onions, making it an excellent candidate for energy storage applications [21]. In addition to such unique structures, these diesel soot carbon may contain a small but significant amount of Sulphur and Nitrogen, which are excellent active sites for Na storage in energy storage devices. With a unique blend of porosity and active sites, diesel soot carbon can be an ideal candidate as electrode material for sodium ion hybrid capacitors.

In this paper, we provide a highly porous, activated diesel soot-derived carbon extracted from automobile exhausts with a high surface area and high conductivity for superior energy performance sodium ion hybrid capacitor. As a result of activation and surface area modification, the as-prepared activated diesel soot carbon electrode has a high specific capacity, rate capability, and extended cycle life. Furthermore, using such high-performance electrodes as both the cathode and the anode, a hybrid capacitor with high efficiency was constructed. The as-prepared sodium ion hybrid capacitor provided the highest energy density and power density, demonstrating how to create wealth from waste and effective procedures for recycling toxic wastewater.

2. Materials and methods

2.1. Synthesis of diesel soot carbon

Diesel soot carbon (DSC) was synthesized by modifying a previous report [22]. The initial stage was to repeatedly clean diesel soot collected from vehicle exhaust to eliminate undesirable petroleum compounds. After washing, 2 g of dry diesel soot was combined with 100 mL of concentrated sulphuric acid (H_2SO_4) and stirred at room temperature for 2 h. The mixture was then stirred for 6 h at 70 °C using a magnetic stirrer with 2 g of potassium permanganate ($KMnO_4$). To avoid MnO_2 precipitation, an ice-cold H_2O_2 solution (10 mL in 1L DI water) was slowly added to the mixture in the last step. The resulting solution was then filtered, pH adjusted to neutral and dried for further use. The dried powder was named DSC.

2.2. Activation of diesel soot carbon

Pure diesel soot carbon from the previous step was used as the starting material to create highly porous carbon. To remove any lumps, the carbon was lightly milled before being combined with potassium hydroxide (KOH), which was five times crushed (the ratio being 1:5). The mixture was pyrolyzed for two hours at 650 °C with a ramping rate of 2 °C/min After carbonization, the sample was repeatedly washed with 0.25 M HCl and DI water until the sample became neutral in order to eliminate excess KOH and neutralize the carbon. Finally, the sample was dried under a vacuum oven overnight, labelled as AcDSC (activated diesel soot carbon) and stored for further experimentation.

2.3. Materials characterization

The crystallinity of the samples was examined using the X-ray diffraction technique (XRD; Cu Ka radiation, Rint 1000, Rigaku, Japan) in the 2θ range of 10° − 90°. The samples' surface texture, elemental composition, and porosity distribution were examined using energy-dispersive X-ray spectroscopy (EDX) and field emission scanning electron microscopy (FESEM, FE-SEM, S-4700, Hitachi, Japan). Its crystallinity at the sub-micron scale was assessed further using field emission transmission electron microscopy (FETEM). The effects of KOH activation on the carbon surface during graphitization and defect formation were investigated using Raman analysis (RAMAN). After prolonged cycling, the impact of electrolytes on electrode surfaces was investigated using X-ray photoelectron spectroscopy (XPS).

2.4. Electrochemical measurement

To conduct electrochemical investigations, CR2032 coin cells were assembled in a controlled ultrapure argon environment. The cells were put up using 1 M $NaPF_6$ in diglyme as the electrolyte, the synthesized materials as the cathode, and metallic Na as the anode, separated by a polypropylene separator. Additionally, the anode and cathode of the full-cell, or hybrid capacitor assembly, were made up of the samples as described below. Ketjen black and teflonized acetylene black were combined with 5 mg of active material to create the cathode materials (TAB-2). Before making the cells, the resultant mixture was compressed onto a stainless-steel current collector and dried for four hours at 160 °C. Charge-discharge (C-DC) tests were carried out using the WonAtech battery test equipment at various voltage ranges for the cathode and anodes, with current rates ranging from 0.01 to 1 Ag^{-1}. For cyclic voltammetry and EIS studies, an electrochemical analyzer (SP-150, Biologic, France) was employed.

3. Result and discussion

3.1. Structural and morphological characterizations

3.1.1. X-ray diffraction studies (XRD)

The morphological structures of DSC and AcDSC were investigated using X-ray diffraction, as illustrated in Fig. 1**a**. The X-ray diffraction patterns showcase characteristic broad peaks around 24.5° and 23.2°, which can be attributed to (002) and (100) planes of graphitic-like carbon. However, the XRD pattern of AcDSC demonstrates distinct differences compared to DSc suggesting modification in morphological structure with KOH activation. For instance- DSC has a (002) peak at 24.5° with a d-spacing of 3.6 nm. In AcDSC, the (002) peak undergoes a left shift and has an increased d-spacing of 3.8 nm. Moreover, high-intensity peaks are added at lower angles (<10°) for AcDSC, suggesting the formation of the mesoporous structure after KOH activation. However, further investigation is required to confirm this notion.

3.1.2. Electron microscopy (SEM and TEM)

The sample morphologies were further studied using scanning (SEM) and transmission electron microscopy (TEM). In Fig. 1**b,** The SEM images showcase a graphitic structure with interconnected carbon nanoparticles. The particle sizes of these carbon nanoparticles were in the range of 70–80 nm. As observed in XRD analysis, the images showcase a granular mesoporosity in AcDSc. Furthermore, TEM analysis was performed to analyze the interlayer spacing of the samples. Fig. 1**c** shows a d-spacing of 3.48 Å which agrees with the d-spacing values obtained in XRD diffraction patterns. In addition, the selected area diffraction (SAED) pattern also matches well with the crystalline planes obtained in XRD results confirming the semi-crystalline nature of AcDSC (**Fig. S-2)**. Furthermore, the surface's graphitic nature supports a prior study (Ref 11), demonstrating a higher order of graphitization and indicating the possibility of improved electrical conductivity.

3.1.3. Surface area analysis (BET)

Nitrogen adsorption/desorption isotherms were utilized to analyze the effect on DSC's surface area and porosity after KOH activation. In Fig. 2**f,** DSC's BET specific surface area increases significantly from 109 m^2g^{-1} to 966 m^2g^{-1} on KOH activation, with an almost nine times increase. In addition, there is also a noticeable increase in the pore volume from 0.7135 to 1.093 $cm^3\ g^{-1}$. This is due to the reaction of carbon atoms in the active sites with the activator (potassium) and

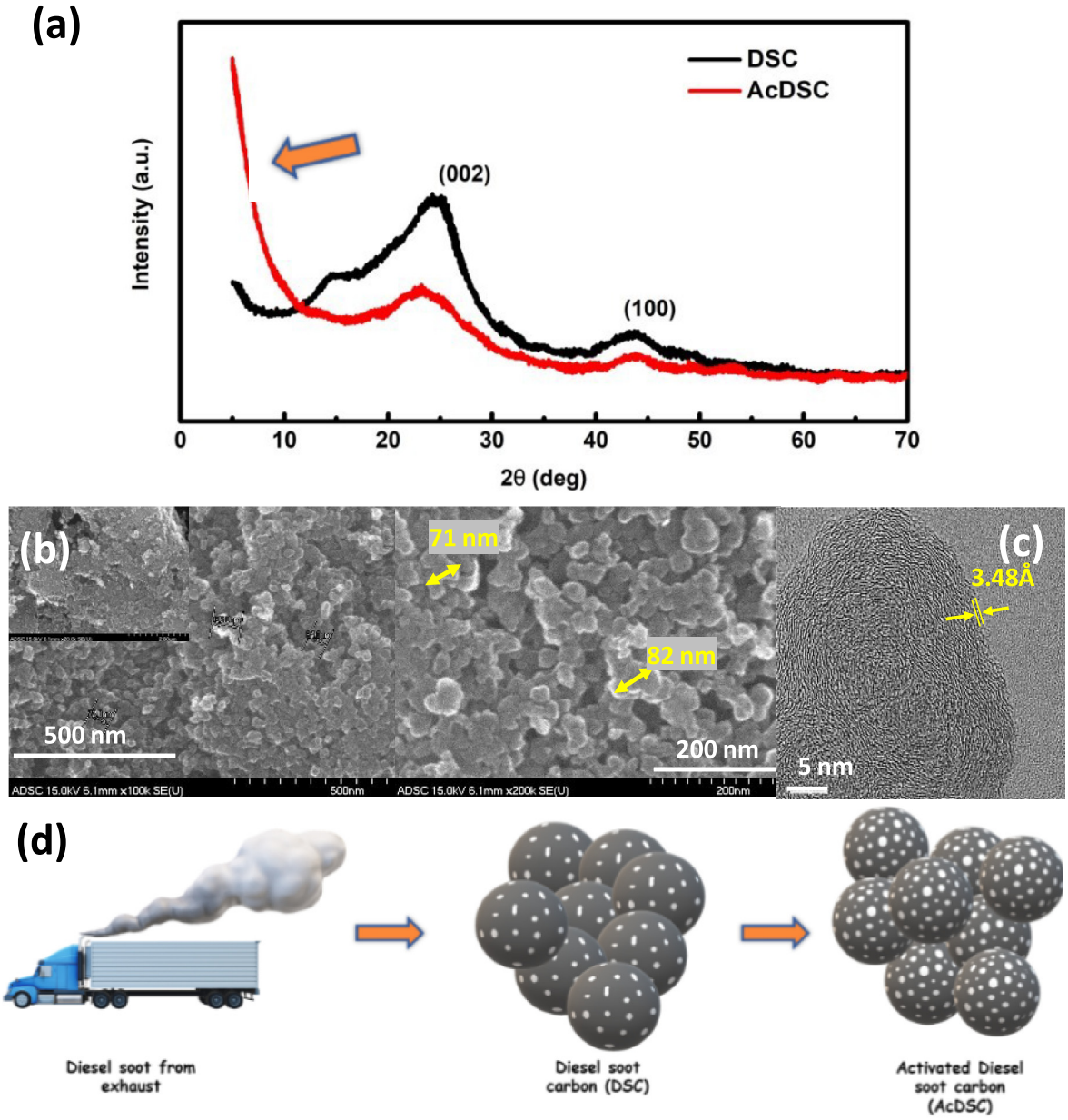

Fig. 1. X-ray diffraction (XRD) images of carbon electrodes (a); Electron microscopy (SEM and TEM) images of AcDSC (b and c); Schematic of synthesis of highly porous carbon (d).

the generation of pore structure at high activation temperatures. Because more ion adsorption sites are available in the cathode due to increased surface area, charge storage capacity will be significantly increased. Although electrochemical tests are needed to confirm it, it is evident from the preliminary analysis that this activation has had a cumulative impact on carbon structure. On the other hand, due to their larger size, increasing pore volume may considerably impact sodium storage. By decreasing sodium diffusion resistance and offering an easy transportation route, an increase in pore volume has improved the sodium transportation process in various cases.

3.1.4. X-ray photoelectron spectrometry (XPS)

Based on XPS analysis, the primary elements present in DSC and AcDSC surfaces were analyzed as carbon and oxygen. Interestingly, nitrogen and Sulphur are present in hydrocarbons such as petroleum products, but both elements were untraceable in XPS survey spectra and in-depth scanning. The carbon and oxygen may have come from hydrocarbons. The C 1 s spectra were fitted with three peaks of C═C (284.6 eV), C-OH (286.7 eV), and O-C═O (287 ~ 289 eV) [23]. In Fig. 2**a and d,** among a comparison of intensities of various carbon peaks, C═C peaks have drastically increased from DSC to AcDSC, indicating higher order of graphitization. This result is in good agreement with the TEM images at higher magnification which shall be further confirmed with Raman analysis. Other than C═C, various C═O and C–OH intensities dropped significantly from DSC to AcDSC. This could happen due to activation at higher temperatures and reduction of carbon atoms, which would cause the carbon to lose its surface oxygen and become graphitized. Due to the improved conductivity of carbon samples caused by stronger graphitization and higher structural integrity during the cycling process, such a change in surface chemistry is

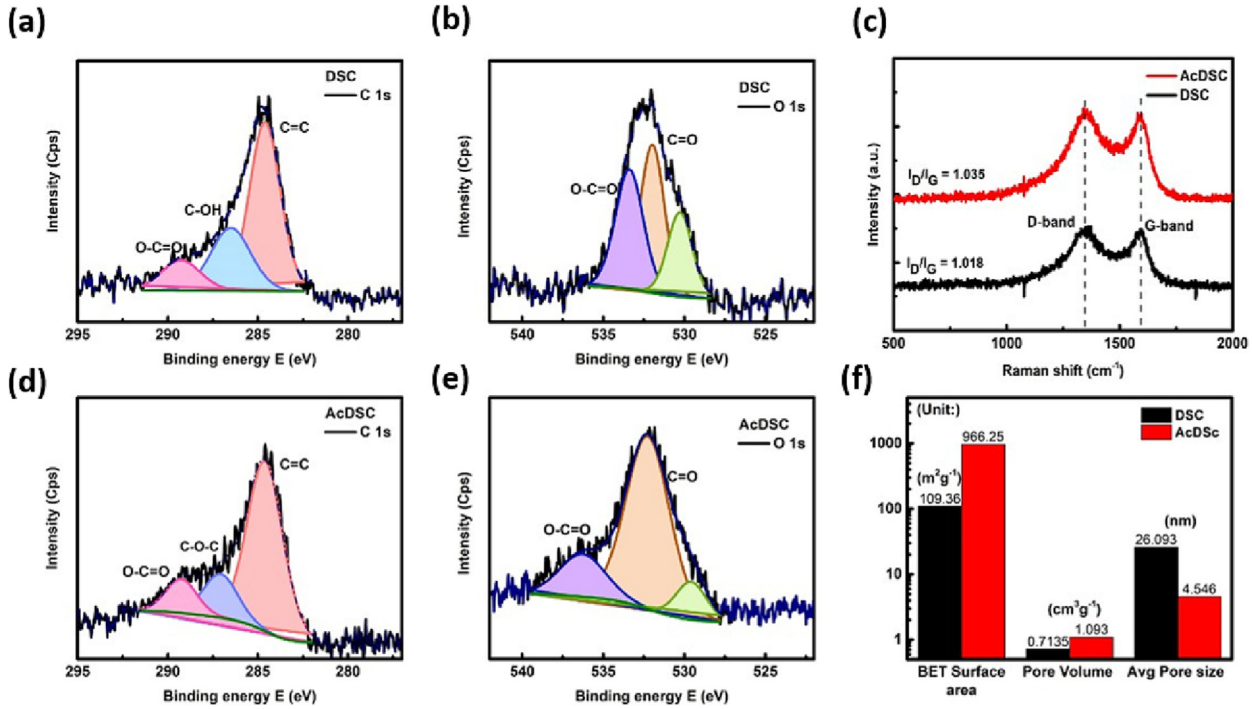

Fig. 2. XPS spectra of DSC electrode (a and b); AcDSC (d and e); Raman spectra with I_d/I_g ratio (c); BET analysis of carbon electrodes using N_2 adsorption isotherm (f);

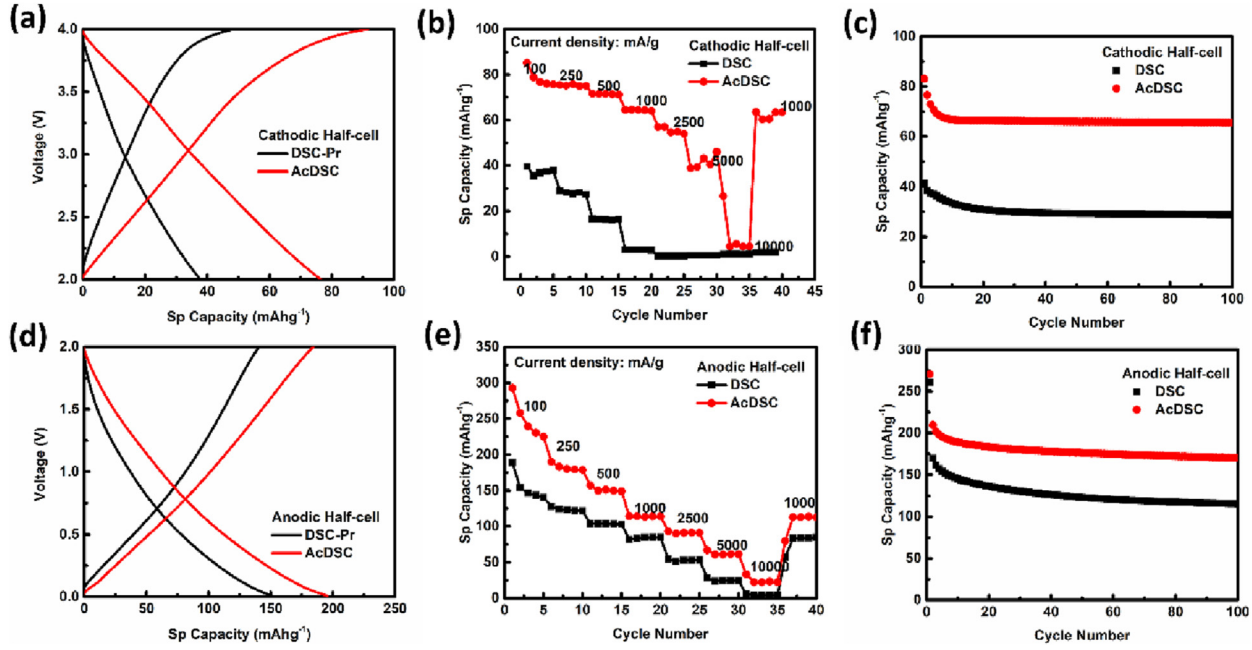

Fig. 3. Half-cell performance of carbon electrode with sodium metal as reference (a and d); Rate performance of carbon electrodes as cathode and anode (b and e); Cycle stability of carbon electrodes as cathode and anode (c and f).

unquestionably advantageous for hybrid capacitor applications. These graphitic characteristics suggest better structural qualities for improved charge storage and electron conductivity during cycling.

3.1.5. Raman spectrometry

Raman spectroscopy was used to analyze the defects and graphitization of AcDSC after KOH activation. The two distinctive peaks in Fig. 2**c** can be attributed to the D and G bands, respectively [24]. The G band occurs due to the first-order scattering of E_{2g} phonon at the Brillouin zone centre of sp^2 carbon atoms. The D band represents the defects or disorders in the sp^2 planar structure [25]. The ID/IG ratio clearly demonstrates the disorder in carbon materials. In this case, KOH activation causes the I_D/I_G ratio to increase, implying the presence of pores or significant defects. These defects should enhance charge storage by increasing the number of active sites.

Contrary to BET data on the increase in surface area, the increase in ID/IG is negligible after activation, suggesting that a graphitic band also rose at the same time as the defect band. Such an increase in the graphitic band may result from increased graphitization upon heating and subsequent activation by KOH, thus inducing defects in the overall system. This suggests an increase in defects and graphitization occurring simultaneously, which could increase diffusivity and electrical conductivity. Further electrochemical studies are required to confirm this idea.

3.2. Half-cell performance

Electrochemical performance of Ac-DSC anode: As mentioned above in the preparation procedure, the electrode materials prepared by the electrode were used as the cathode, along with thin foil of sodium metal (Na) as anode and $NaPF_6$ in diglyme as electrolyte. Al current collectors were used instead of copper in 2032 cells for the working electrode to evaluate cyclic voltammetry (CV) and galvanostatic charge–discharge (GCD) tests at specified current rates. Further, CV curves were drawn in both anodic and cathodic windows of 0.01 – 1.5 V and 1.5 V – 4.0 V vs Na reference, respectively. The current density normalized CVs of the anodic half-cell, or the difference between DSC and AcDSC, are shown in Fig. 4 and exhibited a nearly identical rectangular pattern with minor bumps at roughly 0.47 V versus Na/Na +. In contrast, the critical area of CV normalized for the weight of active material (i.e., current density) has significantly increased, indicating a considerable increase in the surface area available for the electrochemical process and a corresponding increase in charge storage capacity. Conversely, CV, for the cathodic half-cell, has a nearly rectangular voltammogram, indicating higher-order EDLC-type behaviour. A minor bump above 3.5 V suggests a tiny amount of pseudocapacitive behaviour. In addition, the diffusivity of both DSC and AcDSC were calculated from CV at different scan rates in **Fig. S3**, which indicates an order of increase in diffusivity of 5.4×10^{-8} cm^2 s^{-1} for AcDSC from 9.76×10^{-9} cm^2 s^{-1} for DSC by KOH activation.

The carbon electrodes for the GCD were swept between 2.0 and 4.0 V for the cathodic window and 0.01–2.0 V versus $Na|Na^+$ for the anodic window. The carbon electrodes in Fig. 3a's cathodic window demonstrated normal behaviour with a continuous voltage drop that resembled capacitive behaviour. In the instance of DSC, 38 $mAhg^{-1}$ of specific capacity was attained with a smooth slope of the discharge curve at a current rate of 0.1 Ag^{-1}. In contrast, AcDSC was able to reach 78 $mAhg^{-1}$ of specific capacity at the same current density because activation altered the surface and porosity of the material. DSC acting as the anode on the other side of the cell, showed a capacity of 150 $mAhg^{-1}$. Contrarily, a highly porous AcDSC with a larger surface area might give a much higher capacity of 194 $mAhg^{-1}$. The activation of the DSC has increased the specific surface area and porosity, which accounts for the considerable rise in a specific capacity. New voids are formed during activation, providing a significantly increased surface area for cation and anion attachment during electrochemical cycling. The higher rate performance of carbon-based cathodes is well recognized. Rate performance investigation was carried out by increasing current density sequentially from 100 mAg^{-1} to 10 Ag^{-1}, or 100 times the beginning current density in Fig. 3**b and e**, in order to verify the same and the specific capacity at higher density. To test the electrodes' cycle stability in both cathodic and half-cells, a constant current rate of 500 mAg^{-1} was applied for 100 cycles. Similar to different carbon anodes, as seen in Fig. 3**c and f**, the initial capacity was higher for a few cycles before stabilizing at roughly 135 $mAhg^{-1}$ for the DSC electrode. For AcDSC, however, a specific capacity of approximately 187 $mAhg^{-1}$ was attained. Intriguingly, despite the fact that activation tends to increase defects in the carbon surface, resulting in a large number of pores, AcDSC exhibits significantly greater cycle stability than DSC due to the graphitization caused by the heat treatment process for activation. This highlights the fact that a higher degree of graphitization can significantly increase the cycle stability of carbon samples, which is a serious issue for many defect-containing carbon structures. Additionally, a comparable level of stability was attained in the cathodic region as well, with stable capacities of 38 $mAhg^{-1}$ for DSC. In contrast, it could produce a steady capacity of roughly 68 mAhg-1 following activation. Electrochemical impedance is analyzed for both electrode materials before and after cycling for 100 cycles at a constant current rate to better understand the stable cycle performance of both electrodes. Poor conductivity was visible in Fig. 4**b** for the DSC electrode due to reduced graphitization, substantially increasing impedance from 22 to 51 after cycling. Contrarily, the conductivity of AcDSC, which is heavily graphitized as a result of the heating process used during activation, has dramatically increased to 12 and has barely changed beyond 15 even after cycling with the demonstration of larger capacity, which is in good agreement with various previous reports on heteroatoms doped carbon electrodes [26,27]. In summary, the higher degree of graphitization and improved structural integrity of AcDSC reduced the resistance increase during cycling from 130% for DSC to just 25%.

3.3. Full-cell performance

The carbon was used as both a cathode and an anode, connected as a sodium hybrid capacitor with $NaPF_6$ as the electrolyte, to fully use this carbon electrode's potential. Electrode mismatch is one of the main factors contributing to performance deterioration over time and inadequate energy or power density. Individual electrodes operate independently when there is an electrode mismatch, which lowers total performance output. Therefore, using symmetrical capacitors is the best way to eliminate this performance disparity. AcDSC is utilized here as a symmetrical electrode for a sodium hybrid capacitor since it has demonstrated optimal performance as both an anode and a cathode. The current density varied from 100 mAg^{-1} to 10 Ag^{-1} while the connected capacitor was cycled between 0.01 and 4.0 V. It should be mentioned that before being assembled into a full-cell hybrid capacitor, anodes were presodiated in a half-cell configuration with a potential of 0.01 V versus Na/Na + for three cycles.

Additionally, active material mass in cathode: anode ratios of 1:1 demonstrated optimum energy and power performance to maintain charge balance on an electrode. Fig. 5**a** displays the AcDSC's electrochemical performance in both anode and cathode configurations. PF6- ions were stored in positive electrodes with a stable and linear potential increase from 2.0 to 4 V during the charging process. On the other hand, after cycling from 2.0 V to 0.01 V, Na + was stored in an anode with a smooth potential profile. The full-cell hybrid capacitor structure that resulted from linking the electrodes showed a linear charge–discharge curve for a voltage window of 0.01 to 4.0 V. The Ragone plot between energy density and power density is shown in Fig. 5**b**. A maximum energy density of 97 $WhKg^{-1}$ and a maximum power density of 10,000 Wkg^{-1} are seen in the AcDSC symmetrical capacitor. In comparison to other balanced capacitors of the same type, the AcDSC symmetric capacitor performed better overall. Greater porosity and higher order of graphitization, which enable an effective and stable sodium ion storage mechanism, are responsible for enhanced electrode performance. With $1Ag^{-1}$ of current density, the cycle performance of a symmetric AcDSC hybrid capacitor was assessed in Fig. 5**c**. Higher porosity brought on by activation and highly conductive graphitic interlayers made excellent cycle stability possible. With capacity retention of roughly 96% towards the end, this sodium ion capacitor could exhibit exceptional cycle stability of around 50,000 cycles.

Additionally, EIS spectra were taken both before and after the hybrid capacitor was cycled, which showed a negligible increase in resistance because of the remarkably intact surface. In conclusion, positive electrodes should be sufficiently porous to match such output

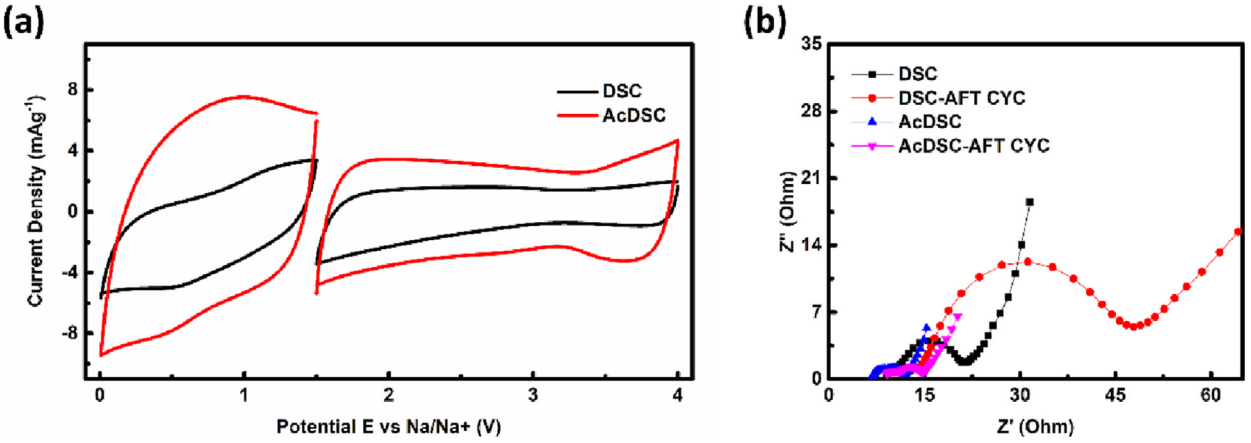

Fig. 4. Cyclic voltammogram (CV) of carbon materials in a cathodic and anodic window (a); Electrochemical impedance spectra of carbon cathodes before and after cycling (b);

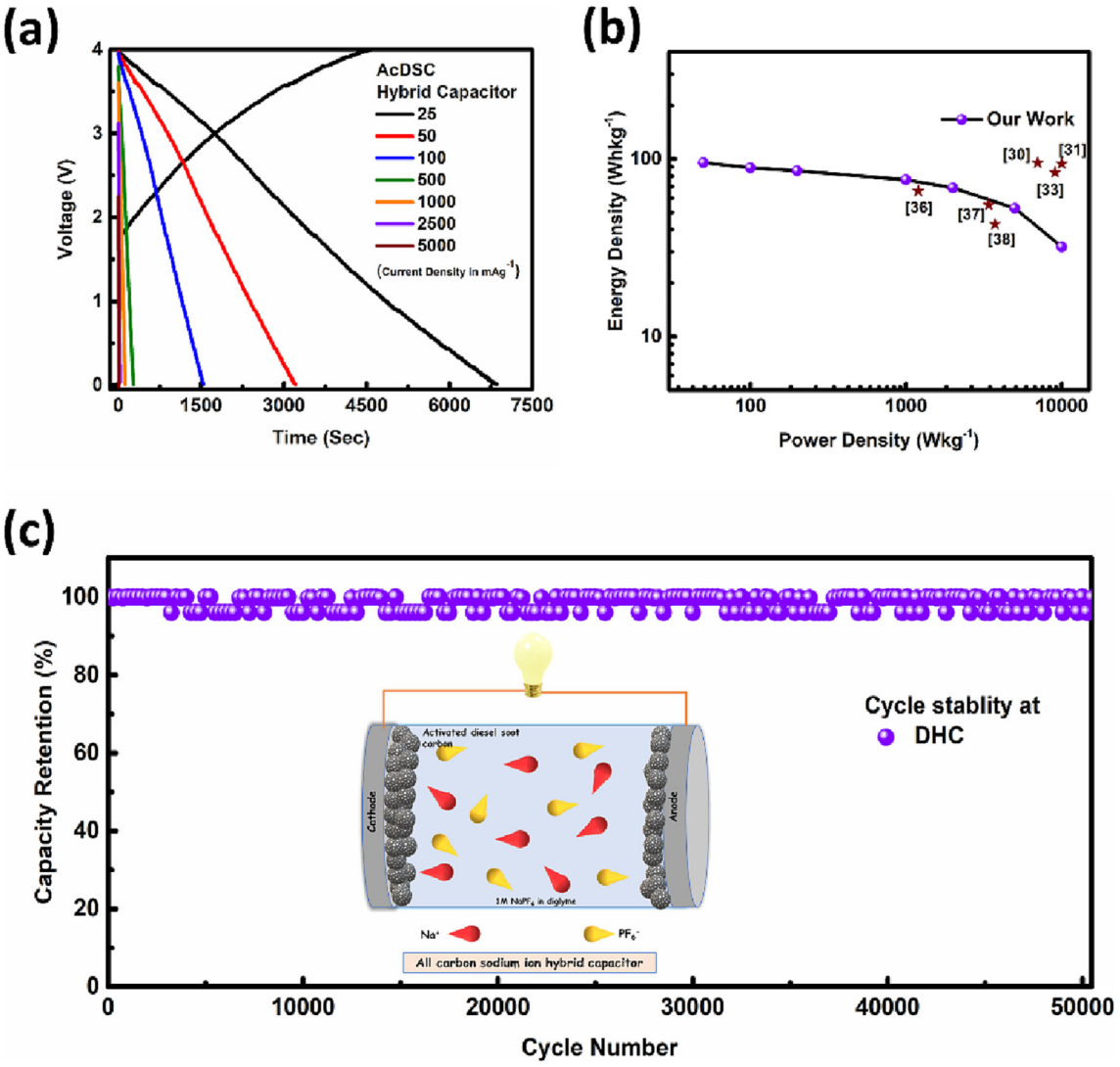

Fig. 5. GCD of Full-cell hybrid capacitor at various current densities (a); Comparison Ragone plot of full-cell performance of carbon hybrid capacitor (b); Cycle stability and schematic of all carbon symmetric sodium ion hybrid capacitor (c);

needs to acquire the best absorption sites and ion diffusion paths. The negative electrode should maintain higher order charge transfer networks and ion-diffusion channels to achieve maximum performance. Even after such optimization, kinetics mismatch in hybrid capacitors

Table 1
Performance comparison of various carbon based electrodes.

Material	Energy Density ($WhKg^{-1}$)	Power density (WKg^{-1})	Cycle number	Reference
N/P dual-doped carbon nanofiber film (NP-CNF)	96	20,000	10,000	[28]
Novel all-organic sodium hybrid capacitor	95	7000	5000	[29]
Biomass-derived porous carbon	94	10,000	2000	[30]
Graphitic mesocarbon microbead	94		3000	[31]
Nteromorpha-derived hierarchical porous carbon (EDHPC)	84	9053		[32]
Coconut shell derived mesoporous carbon (CS-AC)	82		8000	[33]
Watermelon seeds, a bio-waste from watermelons	79	22,500	150,000	[34]
Polyimide as anode	66	1200	1000	[35]
Aromatic polyimide (PI)	65	20,000		[33]
Tailored Polyimide-Graphene Nanocomposite	56	3400	1000	[36]
Activated hard carbon (AHC)	43	3724	50	[37]

with asymmetric electrodes may still occur, resulting in performance loss. In this case, the symmetrical electrode material effectively addresses this issue. Table 1 illustrates how our hybrid capacitor outperforms similar carbon-based electrode addition in a similar segment with better and more promising performance and superior cyclability.

4. Conclusion

In summary, a highly porous graphitized carbon derived from diesel soot was successfully synthesized. Its characteristic porous morphology enabled it to perform better as an anode and cathode. The performance was nearly doubled thanks to the activation technique. Additionally, the carbon electrode demonstrated a high energy density of 97 $Whkg^{-1}$ and a maximum power density of 10,000 Wkg^{-1} when assembled as both an anode and a cathode in a hybrid capacitor. Furthermore, with just a 5% reduction in initial capacity after cycling, the hybrid capacitor's improved performance could be sustained for up to 50,000 cycles and beyond. The mechanism behind the exceptional functioning of all carbon hybrid capacitors was also successfully studied using various characterization techniques. These results indicate an additional way of energy storage using hazardous waste and a clear example of converting waste to wealth.

CRediT authorship contribution statement

Bala Krishnan Ganesan: Conceptualization, Methodology, Formal analysis, Investigation, Software, Visualization, Writing – original draft. **Higgins M. Wilson:** Conceptualization, Methodology, Formal analysis, Investigation, Writing – original draft. **Sangho Park:** Methodology, Formal analysis, Investigation. **Sang Joon Lee:** Funding acquisition, Supervision, Writing – review & editing. **Yun-Sung Lee:** Funding acquisition, Resources, Supervision, Visualization, Validation, Writing – review & editing.

Declaration of Competing Interest

The authors declare that they have no known competing financial interests or personal relationships that could have appeared to influence the work reported in this paper.

Acknowledgement

This work was supported by the National Research Foundation of Korea (NRF) grant funded by the Korean government (Ministry of Science, ICT & Future Planning) (No. RS-2023-00208361). Higgins would like to thank the National Research Foundation of Korea (NRF) for their financial support through the Korean Research Fellowship (Brain Pool Program/2021H1D3A2A01099482).

Appendix A. Supplementary data

Supplementary data to this article can be found online at https://doi.org/10.1016/j.jelechem.2023.117570.

References

[1] M. Armand, J.M. Tarascon, Building better batteries, Nat. 2008 4517179. 451 (2008) 652–657. doi: 10.1038/451652a.
[2] A.S. Aricò, P. Bruce, B. Scrosati, J.M. Tarascon, W. Van Schalkwijk, Nanostructured materials for advanced energy conversion and storage devices, Nat. Mater. 2005 45. 4 (2005) 366–377. doi: 10.1038/nmat1368.
[3] R. Thangavel, A.G. Kannan, R. Ponraj, X. Sun, D.W. Kim, Y.S. Lee, Highly interconnected hollow graphene nanospheres as an advanced high energy and high power cathode for sodium metal batteries, J. Mater. Chem. A 6 (2018) 9846–9853, https://doi.org/10.1039/c8ta00153g.
[4] R. Thangavel, B. Moorthy, D.K. Kim, Y.-S. Lee, Pushing the Energy Output and Cyclability of Sodium Hybrid Capacitors at High Power to New Limits, Adv. Energy Mater. 7 (14) (2017) 1602654.
[5] S. Natarajan, Y.-S. Lee, V. Aravindan, Biomass-Derived Carbon Materials as Prospective Electrodes for High-Energy Lithium- and Sodium-Ion Capacitors, Chem. – An Asian J. 14 (2019) 936–951, https://doi.org/10.1002/asia.201900030.
[6] H. Wang, C. Zhu, D. Chao, Q. Yan, H.J. Fan, Nonaqueous Hybrid Lithium-Ion and Sodium-Ion Capacitors, Adv. Mater. 29 (46) (2017) 1702093.
[7] C. Huang, T. Sun, D. Hulicova-Jurcakova, Wide Electrochemical Window of Supercapacitors from Coffee Bean-Derived Phosphorus-Rich Carbons, ChemSusChem 6 (2013) 2330–2339, https://doi.org/10.1002/CSSC.201300457.
[8] T.E. Rufford, D. Hulicova-Jurcakova, Z. Zhu, G.Q. Lu, Nanoporous carbon electrode from waste coffee beans for high performance supercapacitors, Electrochem. Commun. 10 (2008) 1594–1597, https://doi.org/10.1016/J.ELECOM.2008.08.022.
[9] V. Subramanian, C. Luo, A.M. Stephan, K.S. Nahm, S. Thomas, B. Wei, Supercapacitors from Activated Carbon Derived from Banana Fibers, J. Phys. Chem. C 111 (2007) 7527–7531, https://doi.org/10.1021/JP067009T.
[10] S. Zheng, J. Zhang, H. Deng, Y. Du, X. Shi, Chitin derived nitrogen-doped porous carbons with ultrahigh specific surface area and tailored hierarchical porosity for high performance supercapacitors, J. Bioresour. Bioprod. 6 (2021) 142–151, https://doi.org/10.1016/J.JOBAB.2021.02.002.
[11] L. Feng, B. Yan, J. Zheng, J. Chen, R. Wei, S. Jiang, W. Yang, Q. Zhang, S. He, Soybean protein-derived N, O co-doped porous carbon sheets for supercapacitor applications, New J. Chem. 46 (2022) 10844–10853, https://doi.org/10.1039/D2NJ01355J.
[12] B. Yan, L. Feng, J. Zheng, Q. Zhang, S. Jiang, C. Zhang, Y. Ding, J. Han, W. Chen, S. He, High performance supercapacitors based on wood-derived thick carbon electrodes synthesized via green activation process, Inorg. Chem. Front. 9 (2022) 6108–6123, https://doi.org/10.1039/D2QI01914K.
[13] J. Xiao, H. Li, H. Zhang, S. He, Q. Zhang, K. Liu, S. Jiang, G. Duan, K. Zhang, Nanocellulose and its derived composite electrodes toward supercapacitors: Fabrication, properties, and challenges, J. Bioresour. Bioprod. 7 (2022) 245–269, https://doi.org/10.1016/J.JOBAB.2022.05.003.
[14] H.M. Wilson, S. Rahman AR, T. Garg, N. Jha, Recycling of hazardous diesel soot particles into a high performance solar evaporation device, Appl. Surf. Sci. 487 (2019) 951–961.
[15] Y. Guo, Z. Ristovski, E. Graham, S. Stevanovic, P. Verma, M. Jafari, B. Miljevic, R. Brown, The correlation between diesel soot chemical structure and reactivity, Carbon N. Y. 161 (2020) 736–749, https://doi.org/10.1016/J.CARBON.2020.01.061.
[16] A. Seaton, D. Godden, W. MacNee, K. Donaldson, Particulate air pollution and acute health effects, Lancet (London, England). 345 (1995) 176–178, https://doi.org/10.1016/S0140-6736(95)90173-6.
[17] V. Ramanathan, Global Dimming by Air Pollution and Global Warming by Greenhouse Gases: Global and Regional Perspectives, Nucleation Atmos. Aerosols. (2007) 473–483, https://doi.org/10.1007/978-1-4020-6475-3_94.

[18] V.S.A. Piriya, R.C. Shende, G.M. Seshadhri, D. Ravindar, S. Biswas, S. Loganathan, T.S. Balasubramanian, K. Rambabu, M. Kamaraj, S. Ramaprabhu, Synergistic Role of Electrolyte and Binder for Enhanced Electrochemical Storage for Sodium-Ion Battery, ACS Omega 3 (2018) 9945–9955, https://doi.org/10.1021/acsomega.8b01407.

[19] A.D.H. Clague, J.B. Donnet, T.K. Wang, J.C.M. Peng, A comparison of diesel engine soot with carbon black, Carbon N. Y. 37 (1999) 1553–1565, https://doi.org/10.1016/S0008-6223(99)00035-4.

[20] M. Patel, C.L. Azanza Ricardo, P. Scardi, P.B. Aswath, Morphology, structure and chemistry of extracted diesel soot—Part I: Transmission electron microscopy, Raman spectroscopy, X-ray photoelectron spectroscopy and synchrotron X-ray diffraction study, Tribol. Int. 52 (2012) 29–39, https://doi.org/10.1016/J.TRIBOINT.2012.03.004.

[21] L. Borchardt, M. Oschatz, S. Kaskel, Tailoring porosity in carbon materials for supercapacitor applications, Mater. Horizons. 1 (2014) 157–168, https://doi.org/10.1039/C3MH00112A.

[22] V. Sahu, M. Mishra, G. Gupta, G. Singh, R.K. Sharma, Turning Hazardous Diesel Soot into High Performance Carbon/MnO2 Supercapacitive Energy Storage Material, ACS Sustain. Chem. Eng. 5 (2017) 450–459, https://doi.org/10.1021/ACSSUSCHEMENG.6B01788/SUPPL_FILE/SC6B01788_SI_001.PDF.

[23] J. Kan, H. Wang, H. Zhang, J. Shi, W. Liu, D. Li, G. Dong, Y. Yang, R. Gao, Nitrogen functionalized carbon nanocages optimized as high-performance anodes for sodium ion storage, Electrochim. Acta 304 (2019) 192–201.

[24] G. Jiang, J. Cai, M. Krishnamoorthy, R.A. Senthil, Y. Sun, X. Li, J. Pan, Controlling Morphologies and Structures of PANI@Carbon with Superior Rate Performance for Supercapacitors, ACS Appl. Energy Mater. 5 (2022) 4138–4148, https://doi.org/10.1021/ACSAEM.1C03478/SUPPL_FILE/AE1C03478_SI_001.PDF.

[25] M. Krishnamoorthy, N. Jha, Oxygen-Rich Hierarchical Porous Graphene as an Excellent Electrode for Supercapacitors, Aqueous Al-Ion Battery, and Capacitive Deionization, ACS Sustain. Chem. Eng. 7 (2019) 8475–8489, https://doi.org/10.1021/ACSSUSCHEMENG.9B00233/SUPPL_FILE/SC9B00233_SI_001.PDF.

[26] B. Yan, L. Feng, J. Zheng, Q. Zhang, C. Zhang, Y. Ding, J. Han, S. Jiang, S. He, In situ growth of N/O-codoped carbon nanotubes in wood-derived thick carbon scaffold to boost the capacitive performance, Colloids Surfaces A Physicochem. Eng. Asp. 662 (2023), https://doi.org/10.1016/J.COLSURFA.2023.131018 131018.

[27] B. Yan, L. Feng, J. Zheng, Q. Zhang, Y. Dong, Y. Ding, W. Yang, J. Han, S. Jiang, S. He, Nitrogen-doped carbon layer on cellulose derived free-standing carbon paper for high-rate supercapacitors, Appl. Surf. Sci. 608 (2023), https://doi.org/10.1016/J.APSUSC.2022.155144 155144.

[28] C. Yang, M. Zhang, N. Kong, J. Lan, Y. Yu, X. Yang, Self-Supported Carbon Nanofiber Films with High-Level Nitrogen and Phosphorus Co-Doping for Advanced Lithium-Ion and Sodium-Ion Capacitors, ACS Sustain. Chem. Eng. 7 (10) (2019) 9291–9300.

[29] R. Thangavel, K. Kaliyappan, D.U. Kim, X. Sun, Y.S. Lee, All-Organic Sodium Hybrid Capacitor: A New, High-Energy, High-Power Energy Storage System Bridging Batteries and Capacitors, Chem. Mater. 29 (2017) 7122–7130, https://doi.org/10.1021/acs.chemmater.7b00841.

[30] R. Thangavel, A.G. Kannan, R. Ponraj, M.-S. Park, H. Choi, D.-W. Kim, Y.-S. Lee, High Volumetric Quasi-Solid-State Sodium-Ion Capacitor under High Mass Loading Conditions, Adv. Mater. Interfaces 5 (2018) 1800472, https://doi.org/10.1002/admi.201800472.

[31] P. Han, X. Han, J. Yao, L. Zhang, X. Cao, C. Huang, G. Cui, High energy density sodium-ion capacitors through co-intercalation mechanism in diglyme-based electrolyte system, J. Power Sources 297 (2015) 457–463, https://doi.org/10.1016/j.jpowsour.2015.08.011.

[32] L. Zhuang, Q. Li, S. Chen, X. Hou, J. Lin, In-situ preparation of porous carbon-supported molybdenum dioxide and its performance in the oxidative desulfurization of thiophene, J. Mater. Sci. 49 (2014) 5606–5616, https://doi.org/10.1007/s10853-014-8273-5.

[33] S. Jayaraman, A. Jain, M. Ulaganathan, E. Edison, M.P. Srinivasan, R. Balasubramanian, V. Aravindan, S. Madhavi, Li-ion vs. Na-ion capacitors: A performance evaluation with coconut shell derived mesoporous carbon and natural plant based hard carbon, Chem. Eng. J. 316 (2017) 506–513, https://doi.org/10.1016/J.CEJ.2017.01.108.

[34] R. Thangavel, A.G. Kannan, R. Ponraj, V. Thangavel, D.-W. Kim, Y.-S. Lee, Nitrogen- and Sulfur-Enriched Porous Carbon from Waste Watermelon Seeds for High-Energy, High-Temperature Green Ultracapacitors, J. Mater. Chem. A 6 (36) (2018) 17751–17762.

[35] Q. Zhao, D. Yang, A.K. Whittaker, X.S. Zhao, A hybrid sodium-ion capacitor with polyimide as anode and polyimide-derived carbon as cathode, J. Power Sources 396 (2018) 12–18, https://doi.org/10.1016/j.jpowsour.2018.06.010.

[36] Q. Zhao, D. Yang, C. Zhang, X.-H. Liu, X. Fan, A.K. Whittaker, X.S. Zhao, Tailored Polyimide-Graphene Nanocomposite as Negative Electrode and Reduced Graphene Oxide as Positive Electrode for Flexible Hybrid Sodium-Ion Capacitors, ACS Appl. Mater. Interfaces 10 (2018) 43730–43739, https://doi.org/10.1021/acsami.8b17171.

[37] L. Yin, J. Feng, X. Zhang, L. Li, J. Liu, H. He, Y. Lin, Advanced sodium-ion pseudocapacitor performance of oxygen-implanted hard carbon derived from carbon spheres, J. Mater. Sci. 54 (2019) 4124–4134, https://doi.org/10.1007/S10853-018-3111-9/METRICS.